Pion stars embedded in neutrino clouds

O. S. Stashko,[1,2] O. V. Savchuk,[3,4] L. M. Satarov,[5] I. N. Mishustin,[5] M. I. Gorenstein,[4,5] and V. I. Zhdanov[6]

[1]*Princeton Center for Theoretical Science, Princeton University, Princeton, New Jersey 08544, USA*
[2]*Goethe Universität, Max-von-Laue Str. 1, Frankfurt am Main, 60438, Germany*
[3]*Facility for Rare Isotope Beams, Michigan State University, East Lansing, Michigan 48824 USA*
[4]*Bogolyubov Institute for Theoretical Physics, 03680 Kyiv, Ukraine*
[5]*Frankfurt Institute for Advanced Studies, D-60438 Frankfurt am Main, Germany*
[6]*Taras Shevchenko National University of Kyiv, 03022 Kyiv, Ukraine*

(Received 19 March 2023; accepted 31 May 2023; published 16 June 2023)

We study self-gravitating multipion systems (pion stars) in a state of Bose condensate. To ensure stability of such stars, it is assumed that they are immersed in the lepton background. Two different phenomenological equations of state (EoS) for the pion matter are used, some of them having the first-order phase transition. The model parameters are chosen to reproduce the recent lattice QCD data at zero temperature, but nonzero isospin chemical potential. It is shown that the mass-radius diagrams of pion stars obtained with phenomenological EoS are close to ones calculated in the ideal gas model. We analyze properties of neutrino clouds which are necessary for stabilizing the pion stars.

DOI: 10.1103/PhysRevD.107.114025

I. INTRODUCTION

The cores of astrophysical objects can have sufficiently high densities, at which the nuclear EoS or even the hadron-quark phase transition [1–3] may have observable signatures. Multimessenger astronomy provides important constraints on the properties of strongly interacting matter. In particular, recent observations of gravitational waves from neutron star mergers are used for constraining theoretical models for EoS of stellar matter [4–12]. New data from LIGO-VIRGO-KAGRA detectors are expected to observe new neutron-star mergers [13–15]. New capabilities are associated with the future launch of the LISA mission [16] to provide additional constraints on the nuclear EoS from data of neutron star masses in binary systems. The DUNE and Hyper-Kamiokande neutrino observatories under construction will be able to provide data on the physics of supernova explosions and the physics of neutrinos [17–19]. The prospects of observational technology stimulate interest in exotic astrophysical configurations that can be considered as possible alternatives to the black holes.

Considerable attention is paid to boson star models [20–22], where the Bose-Einstein condensation (BEC) in astrophysical objects is discussed. Systems with BEC were considered in [23–26] as candidates for the dark matter. Unlike these articles, there were attempts to consider BEC within the Standard Model and study models of astrophysical objects made of pions [27–29]. Following [27,30], these objects will be called below as pion stars (PS). At small temperatures these stars contain the Bose condensate of charged pions. The pion condensates have been widely discussed for decades in astrophysics in connection with neutron stars (see, e.g., [31,32] and references therein), they could also be formed in the early Universe [33] and can appear in heavy ion collisions [34,35].

The EoS of the baryon-free strongly interacting matter at low temperature and nonzero isospin chemical potential was recently studied by using lattice quantum chromodynamics (lQCD) simulations [27,33,36,37]. Pions are expected to be the dominant degrees of freedom at such conditions. In particular, the possibility of BEC at isospin chemical potentials close to the pion mass has been demonstrated. The results of these first-principles simulations were used to estimate properties of PS in Ref. [27]. However, characteristics of the external neutrino cloud, necessary for the PS stability, were not considered there.

Different effective models were used to calculate thermodynamic properties of the isospin-asymmetric pion matter, see, e.g., Refs. [38–43]. Recently, the pion matter EoS was considered using two phenomenological models, the effective mass model [44–46] and the mean-field model [47–49]. These models are used in the present paper. Their parameters are chosen to reproduce the lQCD data from Ref. [37]. Both versions, with and without a first-order phase transition (FOPT), are considered. One of our goals is to check whether a presence of the FOPT will

Published by the American Physical Society under the terms of the Creative Commons Attribution 4.0 International license. Further distribution of this work must maintain attribution to the author(s) and the published article's title, journal citation, and DOI. Funded by SCOAP[3].

change the PS properties, in particular, its mass-radius diagram. Also, we pay special attention to stability of PS with respect to weak decays of pions taking into account that this can be achieved only if the star is embedded in the neutrino cloud of galactic size (cf. [27]).

The paper is organized as follows. In Sec. II the phenomenological models for the pion matter EoS and stability conditions in PS are considered. In Sec. III B the contributions of the pion and lepton components of the PS are discussed. Section IV presents calculations of mass-radius diagram for the PS. In Sec. V we consider properties of the neutrino cloud surrounding the inner core of PS, and a short summary in Sec. VI closes the paper.

II. EoS OF ISOSPIN-ASYMMETRIC PION–LEPTON MATTER

Below, we consider isospin-asymmetric pion systems at zero temperature and nonzero isospin chemical potential μ. If interactions are neglected, all pions are at rest and form the pion Bose condensate with $\mu = m_\pi$ where $m_\pi \simeq$ 140 MeV is the pion mass. Within the ideal gas model the pion pressure vanishes, but the energy density is $\varepsilon = m_\pi |n|$, where $n = n_{\pi^+} - n_{\pi^-}$ is the pion isospin density.

A. Ideal gas model for leptons

In a stable macroscopic PS, the Coulomb interactions and weak pion decays should be suppressed. This can be achieved by including charged leptons e and μ as well as neutrinos ν_e and ν_μ [27]. The number densities of charged leptons n_l, pressure p_l, and energy densities ε_l are the functions of the corresponding chemical potentials μ_l. They are determined by well-known formulas of the ideal relativistic Fermi gas ($\hbar = c = 1$):

$$n_l^{\mathrm{id}}(\mu_l) = \frac{g_l}{6\pi^2}(\mu_l^2 - m_l^2)^{3/2}\theta(\mu_l - m_l), \quad (1)$$

$$p_l^{\mathrm{id}} = \int_0^{\mu_l} n_l^{\mathrm{id}}(\mu) d\mu, \quad (2)$$

$$\varepsilon_l^{\mathrm{id}} = \mu_l n_l^{\mathrm{id}} - p_l^{\mathrm{id}}, \quad (3)$$

where $l = (e, \mu)$, $g_l = 2$, and $\theta(x)$ is a theta function. We take the mass values: $m_\mu = 105.6$ MeV and $m_e =$ 0.511 MeV. The same expressions (1)–(3) are valid for massless left-handed neutrinos after replacing $l \to \nu_l$, $g_l \to 1$, and $m_l \to 0$.

B. Phenomenological models for interacting pions

Now we introduce the interaction effects, regarding pions as the only interacting component of the PS. These effects are introduced with two phenomenological models.

1. Effective mass model

First we consider the effective mass (EM) model. It was formulated in Ref. [44] for the pion system at zero chemical potential and later applied for interacting alpha particles in Ref. [50]. Within the EM model pions are represented by a triplet of the interacting scalar fields $\phi = (\phi_1, \phi_2, \phi_3)$ with the effective Lagrangian density

$$\mathcal{L} = \frac{1}{2}(\partial_\mu \phi \partial^\mu \phi - m_\pi^2 \phi^2) + \mathcal{L}_{\mathrm{int}}(\phi^2), \quad (4)$$

where $\mathcal{L}_{\mathrm{int}}$ is the interaction part of the Lagrangian. Below we consider the case of vanishing temperature when all pions are in the Bose condensate. In this case only s-wave $\pi\pi$ interactions play a role and, therefore, the derivative terms in $\mathcal{L}_{\mathrm{int}}$ can be neglected.

In the mean-field approximation one can represent $\mathcal{L}_{\mathrm{int}}$ as a series over the powers of $\delta\sigma = \phi^2 - \sigma$, where $\sigma = \langle \phi^2 \rangle$ is the average scalar density of pions in the grand canonical ensemble. Taking into account only the lowest-order terms, one arrives at the mean-field Lagrangian (see for details Ref. [44])

$$\mathcal{L} \approx \frac{1}{2}[\partial_\mu \phi \partial^\mu \phi - M^2(\sigma)\phi^2] + p_{\mathrm{ex}}(\sigma), \quad (5)$$

where $M(\sigma)$ is the effective pion mass and $p_{\mathrm{ex}}(\sigma)$ is the so-called excess pressure,

$$M^2(\sigma) = m_\pi^2 - 2\frac{d\mathcal{L}_{\mathrm{int}}}{d\sigma}, \qquad p_{\mathrm{ex}}(\sigma) = \mathcal{L}_{\mathrm{int}}(\sigma) - \sigma\frac{d\mathcal{L}_{\mathrm{int}}}{d\sigma}. \quad (6)$$

Following Ref. [44], we use a Skyrme-like parametrization of $\mathcal{L}_{\mathrm{int}}$:

$$\mathcal{L}_{\mathrm{int}}(\sigma) = \frac{a}{4}\sigma^2 - \frac{b}{6}\sigma^3, \quad (7)$$

where a and b are the model parameters which describe, respectively, attractive (at $a > 0$) and repulsive ($b > 0$) interactions between (quasi)particles. At $a = 0$ and $b = 0$ one gets a limiting case of the ideal pion gas. After substituting (7) into (6) one obtains the following expressions for M and p_{ex}:

$$M(\sigma) = \sqrt{m_\pi^2 - a\sigma + b\sigma^2}, \qquad p_{\mathrm{ex}}(\sigma) = -\frac{a}{4}\sigma^2 + \frac{b}{3}\sigma^3. \quad (8)$$

Within the considered model, FOPT may occur in the pionic matter in the case of nonzero positive a. At $T = 0$ this transition takes place between the vacuum and the condensed (liquid) phase. These two phases correspond to zeros of p_{ex}, namely, to scalar densities $\sigma = \sigma_g = 0$ and

TABLE I. The values of interaction parameters in the EM model.

	a	b [MeV^{-2}]	FOPT	W [MeV]
EM I	0	6.2×10^{-4}	absent	0
EM II	1.22	7.8×10^{-4}	exists	−1.28

TABLE II. The values of interaction parameters in the MF model.

	A [MeV · fm^3]	B [MeV · fm$^{3(\gamma+1)}$]	γ	FOPT	W [keV]
MF I	−246.81	536.4	1	absent	0
MF II	224.03	772.36	1/3	exists	−6.1

$\sigma = \sigma_l = 3a/4b$. The binding energy per pion in the condensed phase is nonzero and equals $W = M_l - m_\pi$, where M_l is the pion effective mass in the condensed phase. Using Eq. (8), one obtains

$$M_l = \sqrt{m_\pi^2 - \frac{3a^2}{16b}}. \tag{9}$$

The BEC of cold equilibrium pionic matter occurs at the isospin pion chemical potential $\mu = M_l$. To calculate the pion density n as the function of μ one should solve the system of equations $n = \mu\sigma$, $\mu = M(\sigma)$. The parameters a and b are fitted to the lQCD data [37]. The best fit is denoted by EM II. The corresponding parameters are shown in Table I. The quality of the fit is demonstrated in Fig. 1. To investigate the sensitivity to the FOPT, we present also the results for the purely repulsive pion interaction with $a = 0$ (set EM I). As expected, both FOPT and the bound state of pion matter do not appear in this case (see last two columns of Table I).

Note that in the EM II model the BEC threshold is shifted from the point $\mu = m_\pi$ by $W < 0$. However, this shift is very small, less than 1%, and does not exceed the current accuracy of the lQCD data. Nevertheless, this model predicts the possibility of multipion bound states (pion droplets) which may exist in contact with vacuum [51].

2. Mean field model

The second phenomenological model used in this paper is the mean field (MF) model. This model introduces a density-dependent mean-field potential $U(n)$ which shifts the pion chemical potential μ with respect to its ideal gas value. The pion mass is fixed to its vacuum value. At zero temperature all pions are in the Bose condensate with density $n = n(\mu)$ determined from the equation [48,49]

$$\mu = m_\pi + U(n). \tag{10}$$

The pion pressure $p(\mu)$ is found by integrating $n(\mu)$ over μ.

Following Ref. [52], we assume the Skyrme-like parametrization of the mean-field potential,

$$U(n) = -An + Bn^{\gamma+1}. \tag{11}$$

The parameters A, B, and γ are again found from the best fit of the lQCD data [37]. We consider the cases of a soft ($\gamma = 1/3$) and hard ($\gamma = 1$) repulsion. In the first case the lattice data are better reproduced with positive A (attraction). However, for $\gamma = 1$ a purely repulsive potential is preferable (see Table II). FOPT exists for $A > 0$. The parameters of this transition are found by finding nontrivial solutions of the equation $p(\mu) = 0$. The coefficients of the Skyrme interaction are listed in Table II. Comparison of the EM I, EM II, MF I, and MF II models with the lattice data is presented in Fig. 1(a). As will be seen later, the most important region of the pion EoS for the PS structure is $\mu \approx m_\pi$. This region is shown separately in Fig. 1(b) for the EM I and EM II models.

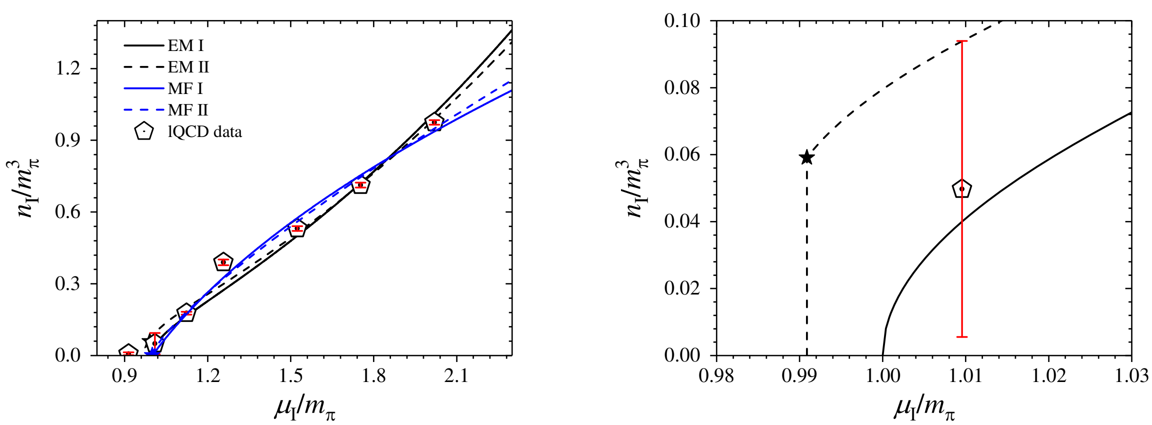

FIG. 1. A comparison of the model results for the pion isospin density n_I as a function of the isospin chemical potential μ_I at $T = 0$ with the lattice data of Ref. [37]. Right panel shows enlarged part of the left lower corner. Star shows position of the BEC threshold state in the EM II model.

III. FULL EoS FOR THE PION STAR MATTER

A. Equilibrium conditions

Stable PS cannot consist of pions only. Indeed, the electric charge of (positively) charged pions must be compensated by (negatively) charged leptons (μ and/or e). The charged pions in the vacuum undergo weak decays. In particular, $\pi^+ \to \mu^+ + \nu_\mu$ proceeds with the lifetime of about 2.6×10^{-8} s. Two other decay modes are $\pi^+ \to e^+ + \nu_e$ and $\pi^+ \to \pi^0 + e^+ + \nu_e$. Muons also decay in the vacuum, e.g., via $\mu^- \to e^- + \bar{\nu}_e + \nu_\mu$. In stable PS the above decays should be suppressed. This suppression can be provided by the Pauli blocking of neutrinos. Thus, in addition to μ^- and e^- which neutralize electric charge, one needs also both ν_μ and ν_e. Therefore, a minimal set of particles in the PS is $(\pi^+, \mu^-, e^-, \nu_\mu, \nu_e)$ or, equivalently, $(\pi^-, \mu^+, e^+, \bar{\nu}_\mu, \bar{\nu}_e)$. We denote this set as $\pi l \nu$.

In our calculations we impose the following constraints: the local charge neutrality,

$$Q = n_I + n_\mu + n_e = 0, \tag{12}$$

and the chemical equilibrium between all constituents:

$$\mu_I = \mu_{\mu^+} + \mu_{\nu_\mu} = \mu_{e^+} + \mu_{\nu_e} \\ = -\mu_{\mu^-} + \mu_{\nu_\mu} = -\mu_{e^-} + \mu_{\nu_e}. \tag{13}$$

At given n_I and μ_I, the lepton chemical potentials and corresponding number densities are found from the conditions (12) and (13), and the ideal gas equation (1). Similar to Ref. [27], we assume the equality $\mu_{\nu_e} = \mu_{\nu_\mu}$, which is motivated by neutrino oscillations. Note that the truncated sets of particle species, like π, πl, or $\pi \nu$, do not satisfy the stability conditions in the PS.

In the case of the FOPT, the transition between the vacuum and the pion Bose condensate takes place at some value of the chemical potential $\mu = \mu_{\rm BC}$ in the interval of pion densities $n < n_{\rm BC}$. To implement FOPT into calculations, we apply the mixed phase construction similar to the Maxwell construction for the liquid-gas phase transition. At $T = 0$ both liquid and gas phases of the phase transition have vanishing pressure and this makes the pionic EoS with the FOPT softer.

B. Components of the pion star

As mentioned above, we treat leptonic components of the PS as mixture of ideal Fermi gases. Their thermodynamic functions are given by Eqs. (1)–(3) with the conditions of electro-neutrality (12) and chemical equilibrium (13).

The complete EoS for the PS matter is then defined by the following set of equations:

$$n_I = n_\mu + n_e, \qquad P = p_\pi + p_\mu + p_e + p_{\nu_\mu} + p_{\nu_e}, \tag{14}$$

$$\varepsilon = \varepsilon_\pi + \varepsilon_\mu + \varepsilon_e + \varepsilon_{\nu_\mu} + \varepsilon_{\nu_e}. \tag{15}$$

Figure 2 show the partial contributions p_i of different system components to the total pressure P as functions of the total energy density ε for the ideal gas (a), EM I (b), and EM II (c) models of the pion EoS. For all three EoS one has the relations $p_\mu < p_e < p_\nu \approx P$. Note that within the ideal gas model the pion pressure vanishes. However, the pion pressure p becomes nonzero in the system of interacting pions, and it changes differently with ε in the EM I and EM II models. Nevertheless, the relation $p \ll p_\nu \approx P$ holds in these models. As a consequence, the sensitivity of $P = P(\varepsilon)$ to the pion matter EoS is very weak. Therefore, it is no wonder that EM and MF models are only slightly deviate from the ideal gas of pions where $p = 0$. In all considered cases the neutrino pressure provides the main contribution compared to other constituents. By this reason, the results for the PS radial profiles are rather robust (see the next section). On the other hand, our calculations show that the size of the pion core for the $\pi l \nu$ star exhibits some sensitivity to the presence of the FOPT.

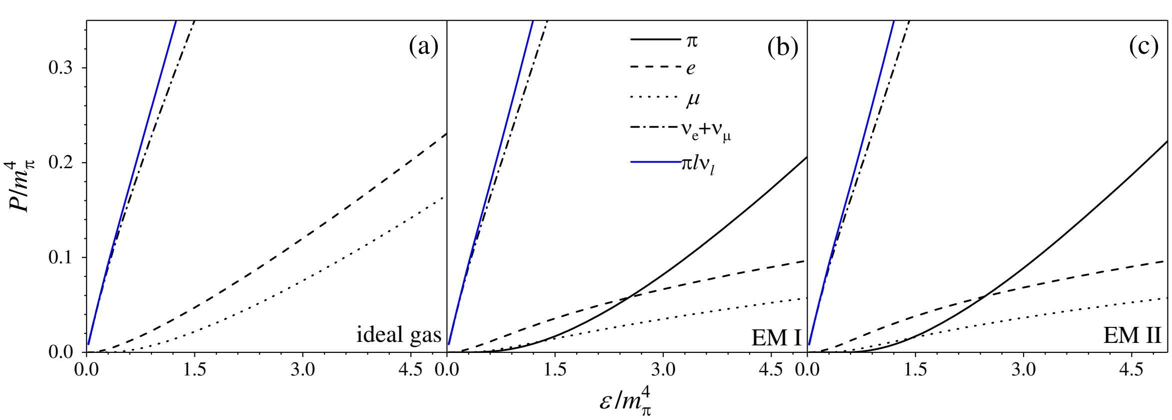

FIG. 2. Partial pressures p_i of different particles species and the total pressure P as functions of the total energy density ε for the ideal gas (a), EM I (b) and EM II (c) models of the pion EoS.

IV. TOV EQUATIONS AND MASS-RADIUS DIAGRAMS

The structure of a static spherical star composed of an ideal isotropic fluid is described by the well-known Tolman-Oppenheimer-Volkoff (TOV) equations which can be written in the form [53,54]

$$\frac{dM}{dr} = 4\pi r^2 \varepsilon(r),$$
$$\frac{dP}{dr} = -G\frac{[\varepsilon(r) + P(r)][M(r) + 4\pi r^3 P(r)]}{r[r - 2GM(r)]}, \quad (16)$$

where G is the gravitation constant, and $M(r)$, $\varepsilon(r)$, and $P(r)$ are, respectively, the integrated mass, energy density and pressure of the fluid at the distance r from the star center.

We solve these equations numerically at given EoS $P = P(\varepsilon)$ defined by Eqs. (14) and (15). The boundary condition assumes $M(0) = 0$ and a certain value of the central pressure $P(0)$. By integrating the Eq. (16) with the conditions at $r \to 0$:

$$M = \frac{4}{3}\pi r^3 \varepsilon(0) + O(r^4), \qquad P = P(\varepsilon(0)) + O(r), \quad (17)$$

one obtains the radial profiles $\varepsilon(r)$. The integration is done outward, up to the surface $r = R_*$, where the densities of pions and charged leptons vanish and neutrinos remain the only matter components. The external neutrino cloud may extend to infinity (see the next section). This is a general feature for the EoS of massless particles.

We define the mass of the PS as $M(R_*) = M_*$. Physical properties of the stars, e.g., the radial profiles of pressure, can be found through their dependence on $\varepsilon(r)$. By considering

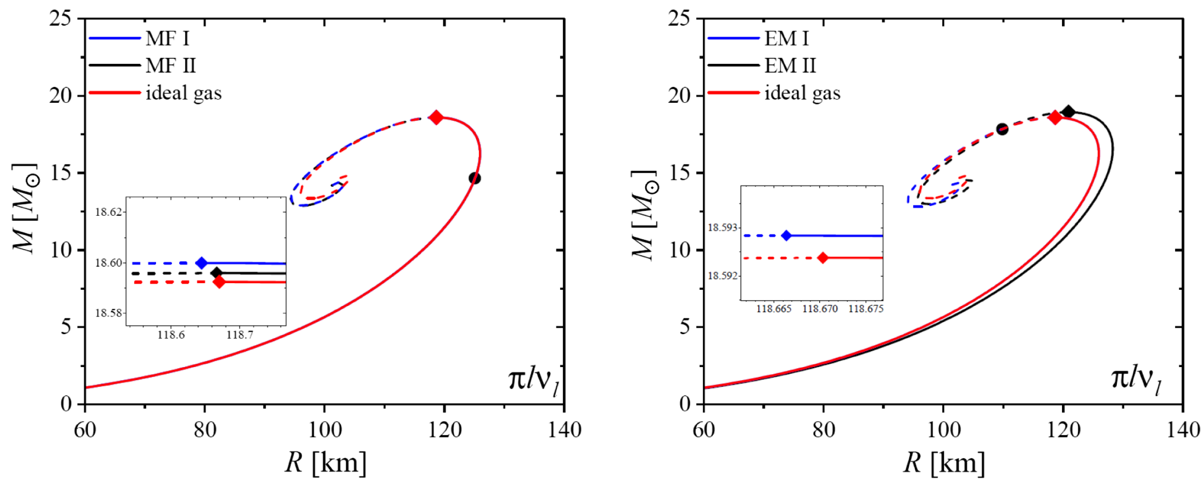

FIG. 3. Mass-radius diagrams of the PS within the MF (left) and EM (right) models. Dashed parts of diagrams correspond to unstable configurations. Inserts represent the results near the states of the maximal mass (shown by diamonds). The black circles represent the points of the phase transition.

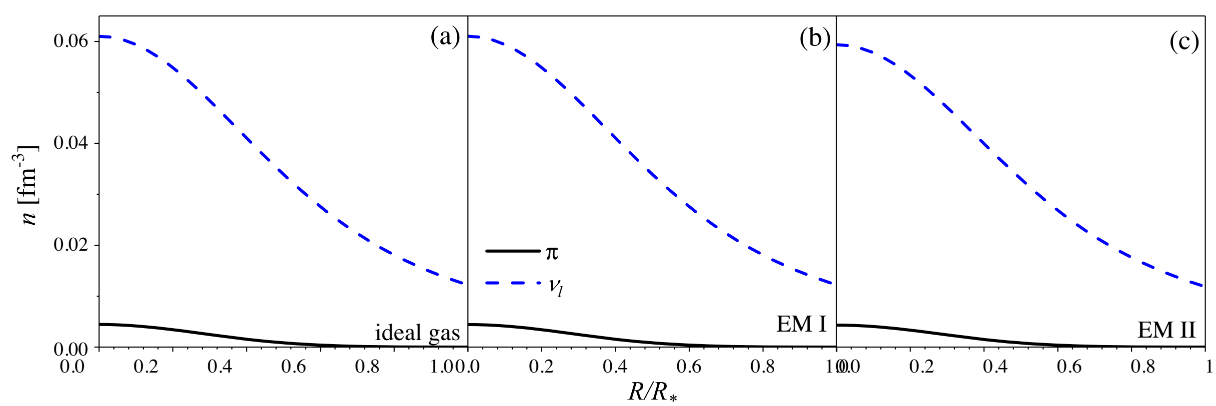

FIG. 4. The particle densities n of different particles species as functions of normalized star radius R/R_* for the ideal gas (a), EM I (b) and EM II (c) models of the pion EoS for the maximal mass configurations. Particle density of muons is equal to zero in all cases.

an ensemble of initial $\varepsilon_c = \varepsilon(0)$ we obtain the line on the $M_* - R_*$ plane. This can be done for different EoS of the pion matter. The mass-radius (MR) diagrams for the PS are presented in Fig. 3. We have compared these diagrams with those calculated in Ref. [27] by using the lQCD data. As expected, the results of [27] for $\pi l \nu_l$ stars nearly coincide with the equilibrium part of the ideal gas diagram in Fig. 3.

As seen from Fig. 3 the ideal pion gas and interacting pion models lead to very similar MR diagrams with maximal masses $M_* \approx 19 M_\odot$ and corresponding radii $R_* = (120 \pm 1)$ km. The EM II model exhibits some sensitivity to the phase transition. As compared to EM I, in this case one gets smaller pion and neutrino pressure, and obtains larger radius ($R_* \approx 121$ km). Thus, there is some sensitivity of the MR diagram to the FOPT in the pion matter. The neutrino cloud exists beyond the pionic core of the PS at $r > R_*$ (see the next section). We checked that implementing non-zero masses of neutrinos leads to finite sizes of neutrino cloud. However, properties of the PS at distances $r < R_*$ are not much influenced by this modification at small enough neutrino masses.

In Fig. 4 we compare the number density profiles of π^+ mesons and neutrinos in PS with maximal masses, using the same EoSs for pions as in Fig. 2. Note that the density profiles of e^- and π^+ coincide due to the charge neutrality. One can see that relative concentrations of pions do not exceed 10% at any radius.

V. PROPERTIES OF STELLAR NEUTRINOSPHERE

In this section we discuss properties of the neutrino cloud surrounding the PS inner core with radius R_*.[1] We do not discuss dynamical processes leading to formation of PS and assume that the radial structure of the final static star (the core + cloud) is given by the solution of the TOV equations (16).

As mentioned above, we define the boundary of the inner core as the radius where densities of pions and charged leptons vanish. Similar to [27], our calculations show that muons do not appear $[\mu(r) < m_\pi + m_\mu]^2$ in the PS even for states with maximal core mass M_*. In accordance with the chemical equilibrium condition, the boundary chemical potential of neutrino equals $\mu_* = m_\pi + m_e \simeq 140.5$ MeV. Corresponding number- and energy densities of neutrino (both flavors) at zero temperature can be calculated as

$$n_* = \frac{\mu_*^3}{3\pi^2} \simeq 0.0122\ \mathrm{fm}^{-3}, \qquad \varepsilon_* = \frac{\mu_*^4}{4\pi^2} \simeq 1.29\ \mathrm{MeV}\cdot\mathrm{fm}^{-3}. \tag{18}$$

Note that these densities can be regarded as the threshold values, above which the pion condensate can be formed inside the cold neutrino matter (see, e.g., Ref. [55]).

Below we consider the state with maximal mass of inner core, $M_* \equiv M(R_*)$ and disregard pion interactions. In this case, the numerical solution of the TOV equations gives $R_* \simeq 120$ km, $M_* \simeq 19 M_\odot$. The calculation shows that the values μ_* and n_* are, respectively, about 64% and 26% of the corresponding central values.

Using the TOV equations, we have checked that at $r > R_*$ the energy density decreases (approximately) inversely proportional to r^2:

$$\varepsilon = \frac{\mu^4}{4\pi^2} \simeq \varepsilon_* \left(\frac{R_*}{r}\right)^2. \tag{19}$$

Formally, this corresponds to the linear increase of the neutrino cloud mass with values $M - M_* \propto (r - R_*)$. However, these relations should be modified at large r due to nonzero neutrino rest mass m. Deviations from ultrarelativistic approximation $\mu \gg m$ occur above some maximal radius, $r \gtrsim r_{\max}$. The latter can be estimated by substituting $\mu = m$ into Eq. (19). Then one obtains

$$r_{\max} \sim R_* \left(\frac{\mu_*}{m}\right)^2. \tag{20}$$

One can consider this radius as a size of the neutrino cloud. Choosing $m = 1$ eV (this does not contradict current observations) one obtains the estimate $r_{\max} \sim 2.4 \times 10^{18}$ km $\simeq 2.5 \times 10^5$ ly and mass $M \sim 10^{17} M_\odot$. The size $r_{\max}$ is comparable with the size of the dark matter halo of our Galaxy [56], but the mass (cf. also [57]) is of the order of that for the largest known matter concentrations in the Universe.

One should have in mind, that these estimates do not take into account that the TOV equations (16) are not justified at the dilute periphery of the neutrino cloud. Indeed, the local thermodynamic equilibrium, used in derivation of these equations, breaks down when the local Knudsen number, $\mathrm{Kn}(r) = \lambda(r)/r$ becomes larger than unity.[3] Here $\lambda(r)$ is the mean-free path of neutrino at the distance r from the PS center:

$$\lambda(r) = \frac{1.6}{n\langle\sigma\rangle}, \tag{21}$$

[1] It is obvious that the "naked" PS (without an external neutrino cloud) is unstable due to nonzero neutrino flux through the surface $r = R_*$. This in turn leads to the decays of pions at $r < R_*$. In such a process the PS can partially or totally evaporate.

[2] In this section we omit index ν.

[3] In particular, at $\mathrm{Kn} \gtrsim 1$, the pressure tensor of the neutrino cloud becomes anisotropic with different transverse and radial components. Calculating the energy density profiles at such distances requires a dedicated kinetic approach. Presumably, nonequilibrium (dissipation) effects will modify the asymptotic behavior of $\varepsilon(r)$ as compared to (19). At larger radii the neutrino cloud can be described only within a kinetic approach. Nevertheless, we expect that the TOV equations can still be used for rough order-of-magnitude estimates.

where $n = n_{\nu_e} + n_{\nu_\mu}$ is the total neutrino density, and $\langle\sigma\rangle$ is the cross section of the $\nu_e\nu_e$ scatterings averaged over the momentum distributions of neutrinos. Coefficient 1.6 takes into account that the $\nu_e\nu_\mu$ cross section is by a factor of 4 smaller [58] than that for $\nu_e\nu_e$ (at the same center of mass energy squared s of the neutrino pair).

Using the explicit expression for $\sigma(s)$, given in Ref. [58], after averaging over the local momentum distribution of neutrinos, one gets the relations

$$\langle\sigma\rangle = \frac{1}{\pi} G_F^2 \langle s\rangle = \frac{9}{8\pi}(G_F\mu)^2 = \sigma_*\left(\frac{n}{n_*}\right)^{2/3}, \quad (22)$$

$$\sigma_* = \frac{9}{8\pi}(G_F\mu_*)^2 \simeq 3.71\times10^{-40}\ \mathrm{cm}^2, \quad (23)$$

where $G_F \simeq 2.3\times10^{-22}$ cm/MeV is the Fermi coupling constant. Substituting (22) into (21) gives

$$\lambda = \lambda_*\left(\frac{n_*}{n}\right)^{5/3} \sim \lambda_*\left(\frac{r}{R_*}\right)^{5/2}, \quad (24)$$

where $\lambda_* = 1.6/(n_*\sigma_*) \simeq 3.53$ m. Note that a much smaller neutrino mean free path, about 37 cm, is obtained at the PS center. The resulting Knudsen number $\mathrm{Kn} \sim \mathrm{Kn}_*(r/R_*)^{3/2}$, where $\mathrm{Kn}_* \simeq \lambda_*/R_* \sim 3.0\times10^{-5}$. This shows that profiles of energy density, predicted by TOV equations, are reliable only up to the radii $r \lesssim R_*/\mathrm{Kn}_*^{2/3} \sim 10^3 R_* \simeq 1.25\times10^5$ km.

VI. SUMMARY

In the present paper we have considered pion stars defined as the self-gravitating configurations with the pion Bose condensate. The local electric neutrality requires additional constituents to be present along the charged pion condensate. Therefore, electrons and muons are added. However, this is not sufficient to have chemical equilibrium, and both muon and electron neutrinos have to be added as well. The mass-radius diagrams of the PS are calculated by solving the TOV equations for different phenomenological pion EoS. Our calculations show that charged leptons and neutrinos contribute significantly to the pressure and the energy density. This makes the results for the interacting pions to be almost identical to those of the ideal pion gas. This finding provides a robust prediction of the PS mass-radius diagram. Some sensitivity to FOPT still remains in size of the PS inner core.

Whether PS can be considered as realistic astrophysical objects is still an open question. In fact, if we want to limit ourselves to a model of a stationary configuration consisting of pions, leptons and massive neutrinos, we can make ends meet. However, unrealistically large mass within the galactic dimensions makes the existence of such object doubtful. To formulate an astrophysically relevant model, one must either include additional components of nuclear matter (as inside neutron stars), or consider a highly nonstationary configuration, or work outside the Standard Model.

ACKNOWLEDGMENTS

The authors are thankful to Scott Pratt and Horst Stoecker for fruitful comments and discussions. O. S. S. is thankful to Horst Stoecker for the warm hospitality at Frankfurt Institute for Advanced Studies. O. V. S. acknowledges support by the Department of Energy, Office of Science through Grant No. DE-FG02-03ER41259. This work is supported by the National Academy of Sciences of Ukraine, Grant No. 0122U200259. L. M. S. and I. N. M. thank for the support from the Frankfurt Institute for Advanced Studies. M. I. G. acknowledges the support from the Alexander von Humboldt Foundation. V. I. Z. acknowledges partial support from the National Research Foundation of Ukraine (Project No. 2020.02/0073). This work was supported by a grant from the Simons Foundation (Grant No. 1039151).

[1] K. Hebeler, J. M. Lattimer, C. J. Pethick, and A. Schwenk, Phys. Rev. Lett. **105**, 161102 (2010).
[2] S. Gandolfi, J. Carlson, and S. Reddy, Phys. Rev. C **85**, 032801 (2012).
[3] C. Drischler, V. Somà, and A. Schwenk, Phys. Rev. C **89**, 025806 (2014).
[4] T. Dietrich, M. W. Coughlin, P. T. H. Pang, M. Bulla, J. Heinzel, L. Issa, I. Tews, and S. Antier, Science **370**, 1450 (2020).
[5] S. Beloin, S. Han, A. W. Steiner, and K. Odbadrakh, Phys. Rev. C **100**, 055801 (2019).
[6] E. R. Most, L. J. Papenfort, V. Dexheimer, M. Hanauske, and H. Stoecker, Eur. Phys. J. A **56**, 59 (2020).
[7] L. R. Weih, M. Hanauske, and L. Rezzolla, Phys. Rev. Lett. **124**, 171103 (2020).
[8] E. R. Most, L. R. Weih, L. Rezzolla, and J. Schaffner-Bielich, Phys. Rev. Lett. **120**, 261103 (2018).
[9] I. Legred, K. Chatziioannou, R. Essick, S. Han, and P. Landry, Phys. Rev. D **104**, 063003 (2021).
[10] C. Drischler, S. Han, J. M. Lattimer, M. Prakash, S. Reddy, and T. Zhao, Phys. Rev. C **103**, 045805 (2021).

[11] S. Huth, P. T. H. Pang, I. Tews, T. Dietrich, A. L. Fèvre, A. Schwenk, W. Trautmann, K. Agarwal, M. Bulla, M. W. Coughlin, and C. V. D. Broeck, Nature (London) **606**, 276 (2022).
[12] D. Neill, R. Preston, W. G. Newton, and D. Tsang, Phys. Rev. Lett. **130**, 112701 (2023).
[13] V. Baibhav, E. Berti, D. Gerosa, M. Mapelli, N. Giacobbo, Y. Bouffanais, and U. N. D. Carlo, Phys. Rev. D **100**, 064060 (2019).
[14] A. Colombo, O. S. Salafia, F. Gabrielli, G. Ghirlanda, B. Giacomazzo, A. Perego, and M. Colpi, Astrophys. J. **937**, 79 (2022).
[15] B. Patricelli, M. G. Bernardini, M. Mapelli, P. D'Avanzo, F. Santoliquido, G. Cella, M. Razzano, and E. Cuoco, Mon. Not. R. Astron. Soc. **513**, 4159 (2022).
[16] P. Amaro-Seoane, J. Andrews, M. Arca Sedda *et al.*, Living Rev. Relativity **26**, 2 (2023).
[17] B. Abi, R. Acciarri, M. A. Acero *et al.*, arXiv:2002.03005.
[18] K. Abe, T. Abe, H. Aihara *et al.*, arXiv:1109.3262.
[19] M. Mezzetto, J. Phys. Conf. Ser. **718**, 022014 (2016).
[20] F. E. Schunck and E. W. Mielke, Classical Quantum Gravity **20**, R301 (2003).
[21] S. L. Liebling and C. Palenzuela, Living Rev. Relativity **20**, 5 (2017).
[22] E. Braaten, A. Mohapatra, and H. Zhang, Phys. Rev. Lett. **117**, 121801 (2016).
[23] A. Suárez, V. H. Robles, and T. Matos, Astrophys. Space. Sci. Proc. **38**, 107 (2014).
[24] T. Bernal, V. H. Robles, and T. Matos, Mon. Not. R. Astron. Soc. **468**, 3135 (2017).
[25] L. Visinelli, J. Cosmol. Astropart. Phys. 07 (2016) 009.
[26] S. HajiSadeghi, S. Smolenski, and J. Wudka, Phys. Rev. D **99**, 023514 (2019).
[27] B. B. Brandt, G. Endrodi, E. S. Fraga, M. Hippert, J. Schaffner-Bielich, and S. Schmalzbauer, Phys. Rev. D **98**, 094510 (2018).
[28] M. Mannarelli, Particles **2**, 411 (2019).
[29] J. O. Andersen and P. Kneschke, arXiv:1807.08951.
[30] S. Carignano, L. Lepori, A. Mammarella, M. Mannarelli, and G. Pagliaroli, Eur. Phys. J. A **53**, 35 (2017).
[31] A. B. Migdal, A. I. Chernoutsan, and I. N. Mishustin, Phys. Lett. **83B**, 158 (1979).
[32] H. Umeda, K. Nomoto, S. Tsuruta, T. Muto, and T. Tatsumi, Astrophys. J. **431**, 309 (1994).
[33] V. Vovchenko, B. B. Brandt, F. Cuteri, G. Endrődi, F. Hajkarim, and J. Schaffner-Bielich, Phys. Rev. Lett. **126**, 012701 (2021).
[34] V. Begun and M. I. Gorenstein, Phys. Lett. B **653**, 190 (2007).
[35] V. Begun and M. Gorenstein, Phys. Rev. C **77**, 064903 (2008).
[36] B. Brandt, G. Endrodi, and S. Schmalzbauer, Phys. Rev. D **97**, 054514 (2018).
[37] Bastian B. Brandt, Francesca Cuteri, and Gergely Endrodi, arXiv:2212.14016.
[38] P. Adhikari and J. O. Andersen, Phys. Lett. B **804**, 135352 (2020).
[39] P. Adhikari, J. O. Andersen, and M. A. Mojahed, Eur. Phys. J. C **81**, 173 (2021).
[40] L.-y. He, M. Jin, and P.-f. Zhuang, Phys. Rev. D **71**, 116001 (2005).
[41] P. Adhikari, J. O. Andersen, and P. Kneschke, Phys. Rev. D **98**, 074016 (2018).
[42] A. Folkestad and J. O. Andersen, Phys. Rev. D **99**, 054006 (2019).
[43] A. Ayala, A. Bandyopadhyay, R. L. S. Farias, L. A. Hernández, and J. L. Hernández, Phys. Rev. D **107**, 074027 (2023).
[44] I. Mishustin, D. Anchishkin, L. Satarov, O. Stashko, and H. Stoecker, Phys. Rev. C **100**, 022201 (2019).
[45] D. Anchishkin, I. Mishustin, and H. Stoecker, J. Phys. G **46**, 035002 (2019).
[46] O. Savchuk, Y. Bondar, O. Stashko, R. V. Poberezhnyuk, V. Vovchenko, M. I. Gorenstein, and H. Stoecker, Phys. Rev. C **102**, 035202 (2020).
[47] O. S. Stashko, D. V. Anchishkin, O. V. Savchuk, and M. I. Gorenstein, J. Phys. G **48**, 055106 (2020).
[48] V. A. Kuznietsov, O. S. Stashko, O. V. Savchuk, and M. I. Gorenstein, Phys. Rev. C **104**, 055202 (2021).
[49] V. A. Kuznietsov, O. Savchuk, O. S. Stashko, and M. I. Gorenstein, Phys. Rev. C **106**, 034319 (2022).
[50] L. M. Satarov, R. V. Poberezhnyuk, I. N. Mishustin, and H. Stoecker, Phys. Rev. C **103**, 024301 (2021).
[51] I. N. Mishustin and W. Greiner, J. Phys. G **19**, L101 (1993).
[52] D. Anchishkin, I. Mishustin, and H. Stoecker, J. Phys. G **46**, 035002 (2019).
[53] R. C. Tolman, Phys. Rev. **55**, 364 (1939).
[54] J. R. Oppenheimer and G. M. Volkoff, Phys. Rev. **55**, 374 (1939).
[55] H. Abuki, T. Brauner, and H. J. Warringa, Eur. Phys. J. C **64**, 123 (2009).
[56] A. J. Deason, A. Fattahi, C. S. Frenk, R. J. J. Grand, K. A. Oman, S. Garrison-Kimmel, C. M. Simpson, and J. F. Navarro, Mon. Not. R. Astron. Soc. **496**, 3929 (2020).
[57] G. Narain, J. Schaffner-Bielich, and I. N. Mishustin, Phys. Rev. D **74**, 063003 (2006).
[58] E. G. Flowers and P. G. Sutherland, Astrophys. J. Lett. **208**, L19 (1976).